Physiologically Realistic LV Models to Produce Normal and Pathological Image and Phantom Data

Alexander I. Veress, W. Paul Segars, Benjamin M. W. Tsui, *Senior Member, IEEE*, Jeffrey A. Weiss, and Grant T. Gullberg, *Fellow, IEEE*

***Abstract*—The cardiac model of the 4D NCAT phantom was enhanced by incorporating a physiological basis from which to realistically model left ventricular (LV) motion defects. A finite element mechanical model of the LV was developed to simulate deficits in contractile function and to study the effect of ischemia on LV function. The model geometry was based on high resolution CT and MRI data sets of a healthy male subject. The myocardial wall was represented as a transversely isotropic material with the fiber angle varying from -90 degrees at the epicardial surface, through 0 degrees at the mid-wall, to 90 degrees at the endocardial surface. An elastance active contraction model was used to provide fiber contraction. Physiological intraventricular systolic pressure-time curves were used to load the ventricle. These features were incorporated into the 4D NCAT cardiac model through the control points, which are set to move according to the principles that govern the mechanical model. A normal model and two pathologic models were created in order to study the effects of ischemia on cardiac function. In the first pathologic model, a sub-endocardial anterior ischemic region was defined and an NCAT image data set was subsequently produced. A second ischemic model was created with a transmural ischemic region defined in the same location as the sub-endocardial ischemia model. These models were able to demonstrate differences in contractile function between subendocardial and transmural infarcts and how these differences in function are documented in the SPECT images that were produced by the NCAT phantom. As demonstrated in this study the 4D NCAT cardiac model provides a valuable tool for the evaluation of imaging methods that assess cardiac function through measurements of myocardial deformation.**

I. INTRODUCTION

Medical imaging devices and procedures are commonly evaluated through computer simulation techniques. These techniques involve computer-generated phantoms that model the patient anatomy and physiology, and models of the imaging process. Given a model of the imaging process, imaging data of a computer phantom can be simulated as if it were an actual patient. A major advantage to using computer-generated phantoms in simulation studies is that the exact anatomy and physiological functions of the phantom are known, thus providing a gold standard from which to evaluate and improve medical imaging devices and techniques. A vital aspect of simulation is to have a realistic computer phantom modeling the subject's anatomy.

The 4D NURBS-based cardiac-torso (NCAT) phantom (Figure 1) [1-3] was developed to provide an accurate model of the human anatomy and physiology. It includes a realistic model for the cardiac and respiratory motions based on tagged MRI data and respiratory-gated CT data respectively. Both datasets were acquired from normal patients. Combined with accurate models of the imaging process, the 4D NCAT can produce simulated images close to that acquired from actual patients. The 4D NCAT is widely used in myocardial SPECT research to simulate healthy patients and those suffering from coronary artery disease (CAD). Ischemic regions, resulting from a blockage in the coronary arteries, can be defined in the NCAT as low perfusion pie-shaped wedges in the left ventricle (LV) as shown in Figure 1. The motion in this region

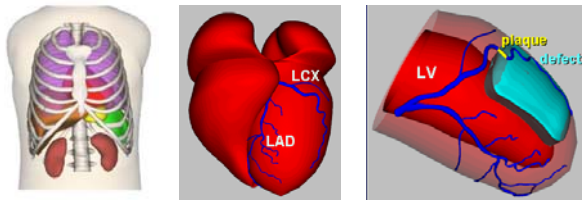

Figure 1. (Left) Anterior view of the 4D NCAT phantom. (Middle) Realistic cardiac model of the 4D NCAT. (Right) Left ventricle model with an anterior myocardial infarction highlighted.

can also be reduced to simulate the altered function of the LV due to the coronary blockage, but currently, there is no physiological basis upon which to base this in the NCAT phantom.

The 4D NCAT phantom was combined with a realistic left ventricle finite element (FE) model in order to produce realistic image data sets in which the effects of ischemia on cardiac function are accurately represented. Three cases have been modeled using an FE representation of the LV that can produce cardiac motion over the entire cardiac cycle. A normal LV model served as a baseline for the evaluation of

This work was supported in part by the National Institutes of Health under Grant RO1-HL50663 and by the Director, Office of Science, Office of Biological and Environmental Research, Medical Sciences Division of the U.S. Department of Energy under contract DE-AC03-76SF00098.

A.I. Veress is in the Department of Bioengineering at the University of Utah, Salt Lake City, UT, 84112 USA

W. P. Segars is in the Department of Radiology at the Johns Hopkins University, Baltimore, MD, 21287, USA

B. M. W. Tsui is in the Department of Radiology at the Johns Hopkins University, Baltimore, MD, 21287, USA

J. A. Weiss is in the Department of Bioengineering at the University of Utah, Salt Lake City, UT, 84112 USA

G. T. Gullberg is with the E. O. Lawrence Berkeley National Laboratory, Berkeley, CA 94720 USA.

changes in cardiac function due to ischemia. Two pathologic models were created in order to study the effects of ischemia on cardiac function as well as produce example image data sets of the modeled ischemia. In the first model, a sub-endocardial anterior ischemic region was defined. A second ischemic model was created with a transmural ischemic region being defined in the same location as the sub-endocardial ischemia model (Figure 2). A simulated myocardial SPECT image data set was produced for each case by combining the FE displacement data with the NCAT phantom.

A. Finite Element Model Generation

A gated high resolution CT image set of a normal male subject acquired on a 32-slice Siemens multi-slice x-ray CT scanner at Johns Hopkins was used as the basis for the cardiac geometry of the finite element model. The patient study consisted of 9 time frames over the entire cardiac cycle. Each time frame consisted of a 512×512×231 image array with a pixel size and slice thickness of 0.421 mm.

The boundaries of the epi- and endocardial surfaces of the left ventricle defined at beginning of diastole were manually segmented from this data set using the software program SURFdriver [4]. SURFdriver was used to display the time-frame images defined at mid-systole and choose points on the inner and outer surfaces of the LV. The segmented points were then used to define a finite element mesh for the LV. The FE model for the LV was surrounded by a soft tether mesh represented by an isotropic hypoelastic constitutive model with relatively soft elastic material properties (modulus of elasticity E=0.30 KPa and the bulk modulus K=0.12 KPa) to provide tethering with the outer edges of the image domain. The tether mesh was fully constrained to eliminate rigid body motion.

B. Passive Material Model

The LV myocardium was represented as a transversely isotropic material with the fiber angle varying from –90° at the epicardial surface, through 0° at the midwall, to 90° at the endocardial surface. The strain energy definition for the transversely isotopic material describes a material that consists of fibers imbedded in an isotropic ground substance. The strain energy function was defined as:

$$W = F_1(\tilde{I}_1, \tilde{I}_2) + F_2(\tilde{\lambda}) + \frac{K}{2}[\ln(J)]^2 . \tag{1}$$

F_1 represents the behavior of the ground substance surrounding the fibers while F_2 represents the behavior of the fibers. The final term represents the bulk behavior of the material. K is the bulk modulus of the material, $\boldsymbol{F}$ is the deformation gradient tensor and J = det($\boldsymbol{F}$). $\tilde{I}_1$ and $\tilde{I}_2$ are the first and second deviatoric invariants of the right Cauchy deformation tensor [5,6]. The scalar $\tilde{\lambda}$ is the deviatoric stretch ratio along the local fiber direction, $\boldsymbol{a}$.

A neo-Hookean form was used to represent the ground substance matrix:

$$F_1(\tilde{I}_1) = \mu(\tilde{I}_1 - 3). \tag{2}$$

where μ is the shear modulus of the ground substance. The stress-stretch behavior for the fiber direction was represented as exponential, with no resistance to compressive load:

$$\begin{aligned} \tilde{\lambda} W_{\lambda} &= \tilde{\lambda}\frac{\partial F_2}{\partial \lambda} = 0, \quad \tilde{\lambda} < 1; \\ \tilde{\lambda} W_{\lambda} &= \lambda\frac{\partial F_2}{\partial \lambda} = C_3\left[\exp\left(C_4\left(\tilde{\lambda}-1\right)\right)-1\right], \ \tilde{\lambda} \geq 1. \end{aligned} \tag{3}$$

The material coefficients C_3 and C_4 scale the fiber stress and control its rate of rise with increasing stretch, respectively. The full passive Cauchy stress tensor is defined as:

$$\boldsymbol{T}^{(p)} = 2(W_1)\boldsymbol{B} + \lambda W_{\lambda}\boldsymbol{a}\otimes\boldsymbol{a} + p\boldsymbol{1} \tag{4}$$

W_1, W_2 and W_λ are strain energy derivatives with respect to I_1, I_2 and λ [6], and $\boldsymbol{B}$ is the left deformation tensor. Details of this constitutive model can be found in Weiss *et al*. [7].

The material properties of the myocardial wall were determined from least squares curve fits of the biaxial test data reported by Guccione et al. [8,9]. The material coefficients for the passive LV were μ = 2.50 KPa, C_3 = 0.39 KPa, and C_4 =20.0. A bulk modulus K of 75.00 KPa was chosen so that the material would be nearly incompressible.

C. Elastance Active Contraction Model

An "elastance" active contraction model [8,9] was added to the passive material model described above thus creating a material model capable of reproducing passive mechanics involved in diastole, as well as the active contraction mechanics of systole. This model is capable of simulating realistic deformations at each point in the cardiac cycle. The total fiber stress T is defined as the sum of the active fiber stress $T^{(a)}$ and the passive Cauchy fiber stress $T^{(p)}$ as shown in the following equation.

$$T = T^{(p)} + T^{(a)}. \tag{5}$$

A detailed description of this constitutive model can be found in the work of Guccione *et al*. [8,9]. The elastance model is a modification of the Hill model in which the Hill equation is scaled by the variable C_t, which governs the shape of the activation curve[9]. The active fiber stress $T^{(a)}$ is defined as

$$T^{(a)} = T_{\max}\frac{Ca_0^2}{Ca_0^2 + ECa_{50}^2}C_t. \tag{6}$$

where T_{max} = 135.7 kPa is the isometric tension under maximal activation and Ca_0 = 4.35 μM is the peak intracellular calcium concentration.

The length dependent calcium sensitivity is governed by the following equation:

$$ECa_{50} = \frac{(Ca_0)_{\max}}{\sqrt{\exp\left[B(l-l_0)\right]-1}}. \tag{7}$$

where $(Ca_0)_{max}$ = 4.35 μM is the maximum peak intracellular calcium concentration, B = *4.75* μm^{-1} governs the shape of the peak isometric tension-sarcomere length relation, l_0 = 1.58 μm is the sarcomere length at which no active tension develops, and $l = lr\times\lambda$ is the sarcomere length which is determined from the fiber stretch λ (deformed

length/reference length) and the sarcomere unloaded length *lr = 2.04* μm.

In the finite element implementation of the "elastance" active contraction model, the activation is governed by the product $T_{max}C_t$ in equation (6). These are then defined as a series of data points specified over the systolic contraction and subsequent relaxation segment of the cardiac cycle. The intraventricular systolic pressure-time curve from Guccione et al. [9] was used over systole, but the diastolic portion of the pressure-time curve corresponding to passive filling was added [10]. The analyses were conducted using the NIKE3D, a non-linear, large deformation finite element package [11]. The deformation results from the analyses were exported to the NCAT model in order to create synthetic myocardial SPECT image data sets.

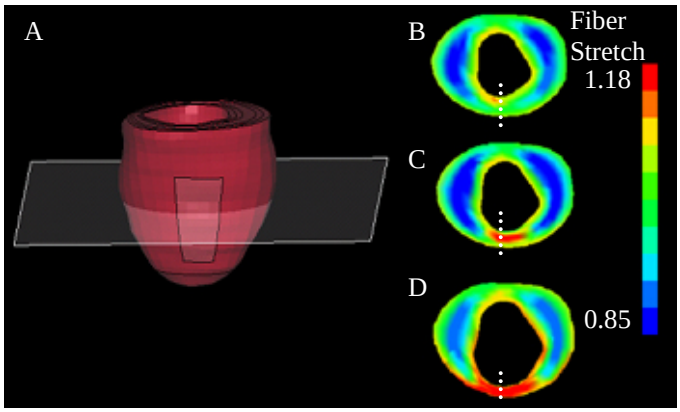

Figure 2. (A) Rectangular light red region of LV indicates location of the ischemia and the cutting plane indicates location of short axis slices. Short axis cross-sections of the normal (B), sub-endocardial (C), and the transmural ischemic (D) models. Ischemic regions show fiber stretch values greater than 1.0 which indicates stretching rather than contraction. Dashed lines indicate location of transmural data in Figure 3.

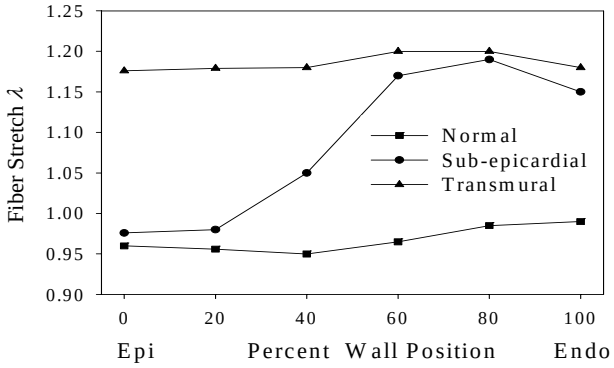

Figure 3. Transmural fiber stretch results through anterior wall section shown in cross-section in Figure 2. Stretch values less than 1.0 indicate contraction.

D. Modeling Regional Ischemia

The ischemic regions were modeled in a similar fashion to the method detailed by Mazhari et al. [4]. The intercellular calcium sensitivity was reduced by increasing $(Ca_0)_{max}$ in equation (6) from 4.35 μM to 7.9 μM in the ischemic regions. The sub-endocardial ischemic region extended through half of the thickness of the myocardium (Figure 2), while the transmural ischemic region encompassed the full thickness of the wall.

E. FE Model Results

The normal model had an ejection fraction of 58%, while the sub-endocardial ischemia model showed a reduced ejection fraction of 55% while the transmural model had an ejection fraction of 48%. The addition of a sub-endocardial ischemic region increased the average transmural stretch by 13% from the contractile value of 0.96 to a tensile value of 1.09. The transmural ischemic region showed 21% increase in average transmural stretch to a value of 1.17 compared with the normal model. The transmural and the normal models showed relatively uniform stretch distributions across the wall (Figure 3). The sub-endocardial results indicate that the non-ischemic wall was contracting against the passive non-contracting ischemic segment of the wall leading to no wall contraction in this region (Figures 2 and 3).

II. NCAT Simulations

A. Methods

The organ models in the NCAT phantom are defined using 3D NURBS surfaces. The size and shape of each NURBS surface model is determined by a set of control points. A surface can be altered by applying affine and other transformations to the control points in order to model anatomical variation or patient motion. The motion of the NCAT heart was modeled by defining time-position curves for each of the control points of the heart surfaces creating time-dependent or 4D NURBS surfaces. The time curves were originally derived from a gated tagged MRI dataset of a normal human volunteer. The 3D positions of the control points over the cardiac cycle were determined from the

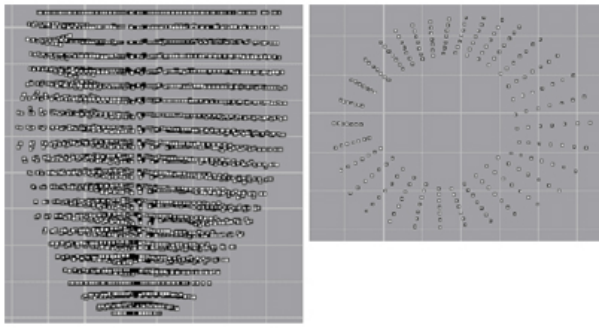

Figure 4. (Left) Long-axis view of the node points defining the FE mesh for the LV at time 0. (Right) Short-axis view of the node points located at the base of the LV. The node points were arranged in a regular order which were used to define the control points for an inner, outer, and five mid-ventricular NURBS surfaces.

motion of the taglines in the dataset.

The FE model of the LV was converted into 4D NURBS surfaces which were then incorporated into the NCAT cardiac model. This was accomplished by using the node points of the FE mesh at time 0 to define the control points for an inner, outer, and five mid-ventricular NURBS surfaces for the LV, (Figure 4). The motion of the node points over the cardiac cycle as determined by the FE analysis were used to define the time-position curves for the control points creating 4D NURBS surfaces for the LV. These surfaces were then used to replace the NCAT's previous LV model.

Using the technique described above, we incorporated the mechanical model for the normal heart as well as the models for ischemia into the 4D NCAT phantom. To demonstrate the use of the improved phantom, a myocardial SPECT simulation was performed by using the different heart models. Using the 4D NCAT, 16 time frame phantoms were generated each modeling the radioactivity concentrations and attenuation distributions in the different organs over the cardiac cycle (1 beat per second). The distribution of radioactivity concentration was set to model the uptake of a typical Tc-99m sestamibi patient study. Each generated 3D phantom was stored in a 128×128×128 array with a pixel size and slice thickness of 0.31 cm. For each heart model, the 16 time frames were averaged to create a phantom of the average beating heart motion for that case.

For each phantom, emission projection data was generated using a realistic parallel projection model simulating an L-configured dual-camera SPECT system equipped with a transmission source. A complete projection dataset over the typical 180° (45° right anterior oblique to 45° left posterior oblique) cardiac arc was generated. The simulations used a projection model that includes the effects of non-uniform attenuation, detector response, and scatter. A low-energy high-resolution (LEHR) collimator with a thickness of 4.1 mm and hexagonal holes with a flat-to-flat size of 0.19 mm was simulated. The 128×128 simulated projection images were collapsed to 64×64 to simulate sampling used in clinical data acquisition.

The emission projection data were reconstructed using the iterative ordered subset expectation maximization (OS-EM) reconstruction method with compensation for attenuation, scatter, and collimator-detector response. The images were reconstructed into 64×64 arrays with 64 slices and a pixel width and slice thickness of 0.63 cm.

B. NCAT Results

Figure 5 shows the endo- and epicardial NURBS surfaces of the LV defined at end-diastole, mid-systole, and end-systole for the normal heart. The motion as determined from the mechanical model was found to compare favorably to that previously defined in the NCAT based on tagged MRI data. Similar 4D NURBS models were created from the FE models for the ischemic heart and incorporated into the 4D NCAT phantom.

Figure 6 shows simulated myocardial SPECT images obtained from the 4D NCAT phantom. Reconstructed short-axis images are shown of the average beating heart motion for each heart model. Figure 6 also shows a profile taken across the anterior region of the LV, the location of the myocardial defect simulated in the ischemic models. The intensity in the reconstructed image across this region can be seen to vary slightly from normal in the simulation with a sub-endocardial defect. More of a difference is seen in the reconstructed image from the model simulating a transmural defect. The simulations agree with the results found in analyzing the FE models.

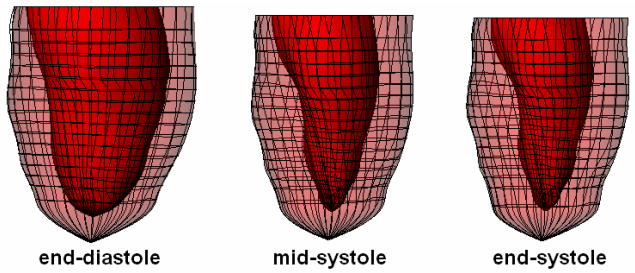

Figure 5. NURBS surfaces defined from the mechanical model developed for the normal heart. Three time points in the cardiac cycle are shown.

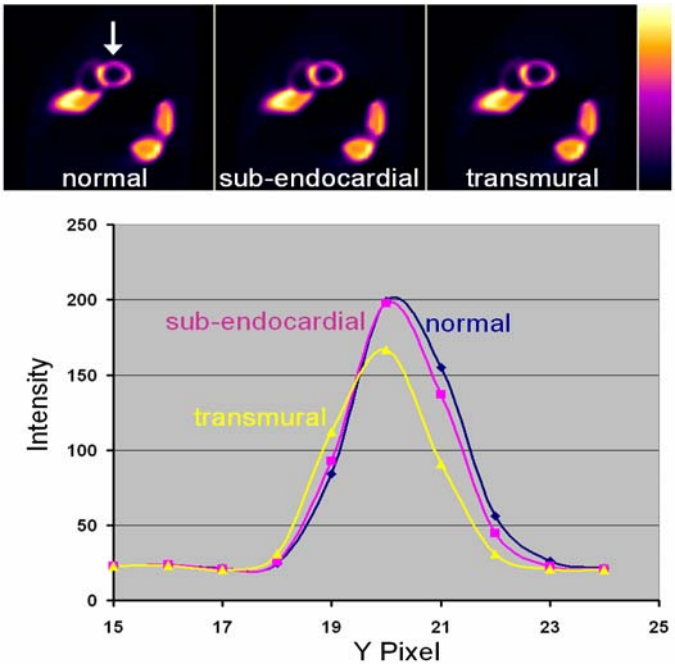

Figure 6. (Top) Reconstructed short-axis slices for the average beating heart motion simulated from the NCAT phantom for the normal and ischemic heart models. (Bottom) Profile taken from the short-axis images across the anterior region (arrow) of the LV. The transmural defect shows the greatest variation to the normal.

IV. Discussion

We developed a finite element model of the left ventricle to simulate deficits in contractile function and to study the effect of ischemia on LV function. The fiber strain results from our normal model were in very good agreement with the predictions of Guccione et al. [9]. The greatest change in fiber strain occurred just outside of the mid-wall location, tapering off to lower contractile values toward the endocardial and epicardial surfaces. However, our values for maximum change in fiber strain during maximum contraction were slightly higher than those in the referenced study (-11% versus -7% for maximum fiber strain referenced to beginning-diastole. This difference is likely due to our use of a realistic geometry as opposed to the cylindrical model used in the Guccione work. Similarly, the overall change in fiber stretch from diastole to systole was consistent with those reported in the literature [12].

The ischemic models showed strain values consistent with those measured in the ischemic dog model [13]. Mazhari et al. measured transmural fiber systolic strains of approximately 14.8% compared with the approximately 9% average sub-endocardial strains and 17% average transmural strains we have reported. The transmural ischemic model fiber strains showed a uniform strain distribution across the wall, similar to that seen in the Mazhari study [13]. Similarly, this region of the LV wall showed a relatively uniform stretch distribution. As mentioned previously, other regions of the LV show a slight increase in contraction at mid-wall. This is likely due to the non-optimal fiber distributions assumed in the models [14-16].

We incorporated the mechanical model into the 4D NCAT phantom to provide a more physiological basis for the cardiac motion of the phantom. With this physiological basis, it is now possible to more realistically simulate motion abnormalities in the LV. With this enhanced ability, the 4D NCAT can provide a valuable tool for the evaluation of imaging methods that assess cardiac function through measurements of myocardial deformation.

References

[1] W. P. Segars, "Development of a new dynamic NURBS-based cardiac-torso (NCAT) phantom., PhD dissertation,," The University of North Carolina, May 2001.

[2] W. P. Segars, D. S. Lalush, and B. M. W. Tsui, "A realistic spline-based dynamic heart phantom,," *IEEE Trans. Nucl. Sci*, vol. 46, 1999.

[3] W. P. Segars, D. S. Lalush, and B. W. M. Tsui, "Modeling respiratory mechanics in the MCAT and spline-based MCAT phantoms," *IEEE Trans. Nucl. Sci.*, vol. 48, pp. 89-97, 2001.

[4] R. Mazhari, J. H. Omens, J. W. Covell, and A. D. McCulloch, "Structural basis of regional dysfunction in acutely ischemic myocardium," *Cardiovascular Research*, vol. 47, pp. 284-93., 2000.

[5] K.-J. Bathe, *Finite Element Procedures in Engineering Analysis*. Englewood Cliffs: Prentice-Hall, 1982.

[6] A. Spencer, *Continuum Mechanics*. New York: Longman, 1980.

[7] J. A. Weiss, B. N. Maker, and S. Govindjee, "Finite element implementation of incompressible, transversely isotropic hyperelasticity," *Computer Methods in Applied Mechanics and Engineering*, vol. 135, pp. 107-128, 1996.

[8] J. M. Guccione and A. D. McCulloch, "Mechanics of active contraction in cardiac muscle: Part I-constitutive relations for fiber stress that describe deactivation," *Journal of Biomechanical Engineering*, vol. 115, pp. 72-81, 1993.

[9] J. M. Guccione and A. D. McCulloch, "Mechanics of active contraction in cardiac muscle: Part II-constitutive relations for fiber stress that describe deactivation," *Journal of Biomechanical Engineering*, vol. 115, pp. 82-90, 1993.

[10] R. M. Berne and M. N. Levy, *Physiology*. St. Louis, MO: Mosby Year Book, 1998.

[11] B. N. Maker, R. M. Ferencz, and H. J.O., "NIKE3D: A nonlinear, implicit, three-dimensional finite element code for solid and structural mechanics," *Lawrence Livermore National Laboratory Technical Report*, vol. UCRL-MA, 1990.

[12] W. Y. Tseng, T. G. Reese, R. M. Weisskoff, T. J. Brady, and V. J. Wedeen, "Myocardial fiber shortening in humans: initial results of MR imaging," *Radiology*, vol. 216, pp. 128-39, 2000.

[13] R. Mazhari, J. H. Omens, R. S. Pavelec, J. W. Covell, and A. D. McCulloch, "Transmural distribution of three-dimensional systolic strains in stunned myocardium," *Circulation*, vol. 104, pp. 336-41., 2001.

[14] T. Arts, K. D. Costa, J. W. Covell, and A. D. McCulloch, "Relating myocardial laminar architecture to shear strain and muscle fiber orientation," *Am J Physiol Heart Circ Physiol*, vol. 280, pp. H2222-9, 2001.

[15] J. Rijcken, P. H. Bovendeerd, A. J. Schoofs, D. H. van Campen, and T. Arts, "Optimization of cardiac fiber orientation for homogeneous fiber strain during ejection," *Ann Biomed Eng*, vol. 27, pp. 289-97, 1999.

[16] J. Rijcken, P. H. Bovendeerd, A. J. Schoofs, D. H. van Campen, and T. Arts, "Optimization of cardiac fiber orientation for homogeneous fiber strain at beginning of ejection," *J Biomech*, vol. 30, pp. 1041-9, 1997.